Neural network-based finite volume method and direct simulation Monte Carlo solutions of non-equilibrium shock flow guided by nonlinear coupled constitutive relations

Gagan Garg (गगन गर्ग)[a], Tapan K. Mankodi (तपन के मंकोड़ी)[b], Esmaeil Esmaeilifar (اسماعیل اسماعیلی فر)[a], Rho Shin Myong (명노신)[a),1)]

[a)] School of Mechanical and Aerospace Engineering and ACTRC, Gyeongsang National University, Jinju, Gyeongnam 52828, South Korea

[b)] Department of Mechanical Engineering, Indian Institute of Technology Guwahati, Guwahati 781039, India

Abstract: For understanding many real-world problems involving rarefied hypersonic, micro-, and nanoscale gas flows, the primary method may be the direct simulation Monte Carlo (DSMC). However, its computational cost is prohibitive in comparison with the Navier-Stokes-Fourier (NSF) solvers, eclipsing the advantages it provides, especially for situations where flow is in the near continuum regime or three-dimensional applications. This study presents an alternate computational method that bypasses this issue by taking advantage of data-driven modeling and nonlinear coupled constitutive relations. Instead of using numerical solutions of higher-order constitutive relations in conventional partial differential equation-based methods, we build compact constitutive relations in advance by applying deep neural network algorithms to available DSMC solution data and later combine them with the conventional finite volume method for the physical laws of conservation. The computational accuracy and cost of the methodology thus developed were tested on the shock wave inner structure problem, where high thermal non-equilibrium occurs due to rapid compression, for a range of Mach numbers from 2 to 10. The simulation results obtained with the computing time comparable to that of the NSF solver showed almost perfect agreement between the neural network-based combined finite volume method and DSMC and original DSMC solutions. We also present a topology of DSMC constitutive relations that allows us to study how the DSMC topology deviates from the NSF topology. Finally, several challenging issues that must be overcome to become a robust method for solving practical problems were discussed.

Keywords: Rarefied and microscale gases; deep neural network; DSMC; constitutive relations; finite volume method; shock wave structure

[1)] Corresponding author: Tel: +82-55-772-1645. Email: myong@gnu.ac.kr.

I. INTRODUCTION

In fluid dynamics, constitutive relations play a crucial role in describing the thermo-fluidic behavior of a flow subjected to certain thermodynamic forces like spatial gradients of velocity or temperature. These relations, in combination with the conservation laws of mass, momentum, and energy, provide the governing equations applicable to a physical flow situation. For any application, the solution of these governing equations with imposed initial and boundary conditions provides the physical representation of the system.

The most widely used set of constitutive relations in fluid dynamics are the Navier-Stokes and Fourier (NSF) relations (linear in nature). A vital assumption in these relations is that the flow constitutes a near-local thermal equilibrium (LTE). This assumption does not hold for applications that are not near LTE. With recent advancements in science and technology, various applications have surfaced where the flow exhibits the presence of thermal non-equilibrium. These include the motion of a gas in rarefied, micro-scale [1-7], and hypersonic flow conditions [8-10], electron transport in semiconductor devices [11, 12], and non-Newtonian viscoelastic fluids (like polymer solutions, lubricant fluids, and complex fluids) [13, 14]. The solution for these applications requires a governing equation that consists of higher-order constitutive relations.

These flow situations require a set of governing equations comprising a new set of constitutive relations or gas kinetic equations. The most general governing equation capable of providing the correct solution for flows with the presence of thermal non-equilibrium is the Boltzmann kinetic equation (BKE). The BKE for a monatomic gas can be written as,

$$\left(\frac{\partial}{\partial t}+\boldsymbol{v}\cdot\nabla\right) f\left(\boldsymbol{v},\boldsymbol{r},t\right)=C\left[f,f_2\right], \tag{1}$$

where $f\left(\boldsymbol{v},\boldsymbol{r},t\right)$ and $C\left[f,f_2\right]$ represent the distribution function in terms of the particle velocity, the particle position, and time, and the Boltzmann collision integral, respectively. The direct analytical and numerical solutions of BKE are complex due to the Boltzmann collision integral term.

An alternative to this approach involves solving BKE using the computational methodology; for example, direct simulation Monte Carlo (DSMC). In the DSMC method, the molecular behavior of gases is simulated directly by decomposing the motion of the particles into two steps, i.e., deterministic movement and stochastic collision via Monte Carlo [15-17], with the assumption of one simulated particle representing a large number of real particles. The DSMC method is a pure particle method that is not based on any partial differential equations (PDEs). Mathematically, the solution of DSMC converges to the solution of the BKE, where the gas experiences binary collisions of gas particles. However, utmost care must be taken when choosing the critical computational parameters, such as the time step, the cell size, and the number of DSMC particles [15-19]. Since its inception, DSMC has evolved into a primary workhorse for obtaining the numerical solution of the BKE and has been routinely applied to various flow problems of scientific and technological interest.

A critical issue with DSMC is that it is generally computationally expensive, prohibitively so, especially in the regime near the continuum limit and in three-dimensional flow problems [15-19]. The problem is that DSMC requires the tracking of a large number of statistically representative particles. To address this issue, in recent years various researchers have focused on developing hybrid NSF-DSMC solvers [20-23]. Since these solvers still employ DSMC for at least some part of the computational domain, these solvers still suffer a higher computational cost compared to conventional CFD methods. In parallel, various researchers have worked on the critical issue with the direct solution of BKE, i.e., the collision integral, and have attempted to create a simplified model for this term. Among these, the Bhatnagar-Gross-Krook (BGK) [24], Shakhov-BGK [25], and ellipsoidal statistical BGK (ES-BGK) [26] present linearized or simplified Boltzmann model equations.

Instead of the aforementioned particle-based methods, the PDE-based methods would propose a new set of equations using higher-order constitutive relations. Taking this approach, various researchers have presented a new set of equations called the extended or generalized hydrodynamic equations. These include the Burnett equations [27-29], the Grad equations [30], and the regularized moment equations (R-

13 [31] and R-26 [32]). In another study, based on Eu's generalized hydrodynamic equations [33], Myong [1, 3, 5, 6, 7, 34, 35] developed the nonlinear coupled constitutive relations (NCCR) in algebraic form.

Estimating macroscopic properties using methods based on hydrodynamic equations is computationally efficient, but has a crucial disadvantage in that the predicted values of the macroscopic properties are less accurate than the ones predicted using full kinetic methods. Consequently, the development of a computationally comparable (to conventional NSF solvers) solution methodology for non-equilibrium gas flows remains a prime concern.

Specifically, it is necessary to develop an innovative technique that can solve the key shortcoming of the DSMC method, i.e., the high computational cost that results from the solution methodology implemented in DSMC, i.e., being a stochastic simulation process. One computationally efficient scenario could be to solve the conservation laws in conjunction with the nonlinear coupled constitutive relations directly obtained from the DSMC data.

The origin of this novel idea can be traced back to Myong's 1999 article in the *Physics of Fluids* in which it was stated that "*if a method in which the constitutive relations are stored as a separate database or an operator-splitting method is adopted, the additional computational cost can be trivial compared with the Navier-Stokes relations*." [1, p. 2800].

In this study, instead of using numerical solutions of higher-order constitutive relations in conventional algebraic or differential form, *we use DSMC data to build a separate database for constitutive relations (CR) in advance and later combine it with the conservation laws (CL), which are fundamental laws of physics*. It should be noted that this new method is the third way to solve gas flows in thermal non-equilibrium (PDE for CL and data extracted from DSMC for CR), which distinguishes it from the existing methods: PDE-based CFD method (PDE for both CL and CR) and pure particle method (DSMC for both CL and CR).

In recent years, a new statistical technique based on data-driven modeling has proved to be a useful tool in various fields. It has also piqued the interest of researchers working in fluid dynamics. In the field of turbulence, numerous researchers have employed this data-driven technique to develop models for the

Reynolds-averaged Navier-Stokes (RANS) utilizing high-fidelity numerical and experimental data [36-39]. Recently, this data-driven technique has attracted the attention of researchers working in rarefied gas dynamics.

Zhang and Ma [40] employed the PDE-FIND algorithm [41] to derive the governing equations of various flow situations using macroscopic property data from DSMC. Xing et al. [42] used gene expression programming to derive the governing equation for various fluid flow situations using the macroscopic properties and their gradients predicted by DSMC as the input data. Yao et al. [43] and Zhao et al. [44] developed machine learning (ML) models using a randomized tree algorithm, where the mapping was carried out between the data of macroscopic properties and their gradients from the unified gas kinetic scheme (UGKS) and the NSF solution. Nair et al. [45] developed a deep neural network (DNN) model mapping the gradients of macroscopic properties from DSMC using similar gradients from NSF.

The current work exploits the advantages of constitutive relations, i.e., developing a DNN model (one of the ML algorithms) for the constitutive relations using the DSMC data. This model can then act as the new higher-order constitutive relations for the conservation laws, allowing the development of a computational methodology that predicts the DSMC results with a computational cost comparable to the conventional NSF solvers. The choice of the DNN model over less complex techniques like simple curve fitting, regressions, or least-square to develop the constitutive relations emanates from the fact that the one-dimensional shock problem has a high degree of non-linearity and modeling such a phenomenon by using routine curve-fitting/least-square methods will cause the model to lose generality, which prevents us from achieving our critical goal, i.e., a single model that works for all the intermediate Mach numbers and whose DSMC solution is not a part of training the DNN model.

To verify the essence of the new method, we first consider the NCCR model for a monatomic gas developed by Myong and his collaborators [1, 5, 7, 34, 35] in conjunction with conservation laws. We generate the NCCR data by numerically solving the NCCR model, develop a DNN model for the constitutive relations from the NCCR data, and finally combine the DNN model with the finite volume method (FVM) of conservation laws. By comparing this FVM-NCCR-ML solution with an original

FVM-NCCR solution, we can verify the accuracy of the FVM-NCCR-ML method. Further, we construct a topology of DSMC constitutive relations, which allows us to study how the DSMC topology deviates from the NSF topology when the flow is away from local thermal equilibrium.

While various situations can cause a gas flow to become non-equilibrium (some of which are compression, expansion, and velocity shear), the current study focuses on FVM-ML algorithms (FVM-NCCR-ML and FVM-DSMC-ML) for the one-dimensional compressive shock structure problem because of its simplicity and importance for gases in high non-equilibrium states.

II. CONSERVATION LAWS AND CONSTITUTIVE RELATIONS

Any conventional numerical technique shares the same physical laws of conservation which for mass, momentum, and energy are as follows [1, 18, 19, 35],

$$\frac{\partial}{\partial t}\underbrace{\begin{bmatrix}\rho\\ \rho\mathbf{u}\\ \rho E\end{bmatrix}}_{\substack{Conserved\\ Variable}} + \nabla\cdot\underbrace{\begin{bmatrix}\rho\mathbf{u}\\ \rho\mathbf{u}\mathbf{u}+p\mathbf{I}\\ \left(\rho E+p\right)\mathbf{u}\end{bmatrix}}_{\substack{Inviscid\\ Flux}} + \nabla\cdot\underbrace{\begin{bmatrix}0\\ \boldsymbol{\Pi}\\ \boldsymbol{\Pi}\cdot\mathbf{u}+\mathbf{Q}\end{bmatrix}}_{\substack{Viscous\\ Flux}} = 0\ . \tag{2}$$

Here ρ is the density, $\mathbf{u}$ is the fluid velocity, p is the pressure, and E is the total energy. The following relations of the equation of state (EOS) and E are also assumed (T, γ, and R_g are the temperature, the specific heat ratio, and the gas constant, respectively);

$$p=\rho R_g T,\ E=\frac{p}{\rho(\gamma-1)}+\frac{1}{2}\mathbf{u}\cdot\mathbf{u}\,. \tag{3}$$

It should be mentioned here that the perfect EOS is satisfied in DSMC solutions [16]. It has been shown in previous works [2, 5, 7, 18, 19] that this set of equations (2) is an exact consequence of the original Boltzmann kinetic equation (1). Only after some approximations like the linear Navier and Fourier constitutive relations are introduced into the viscous shear stress ($\boldsymbol{\Pi}$) and the heat flux ($\mathbf{Q}$) in (2); do they become approximate, thereby valid only near LTE.

The key difference between various methodologies is how the constitutive relations for the viscous stress tensor and heat flux vector are modeled. The NSF set of equations (widely applied to solve in many

applications) employs a linear approximation (μ, k being the viscosity and thermal conductivity, respectively), i.e.,

$$\begin{aligned} \mathbf{\Pi}_{NSF} &= -2\mu\left[\nabla\mathbf{u}\right]^{(2)}, \\ \mathbf{Q}_{NSF} &= -k\nabla T. \end{aligned} \tag{4}$$

Here, μ is the viscosity, k is the thermal conductivity, and the symbol $\left[\mathbf{A}\right]^{(2)}$ stands for the traceless symmetric part of a tensor $\mathbf{A}$. If the conservation laws (2) are solved together with these linear constitutive relations for non-equilibrium gas flows, the predictions of macroscopic properties will be valid only near LTE.

Thus, for the case of non-equilibrium flows, the constitutive equations for the two undetermined variables, i.e., viscous stress tensor, and heat flux are derived by first differentiating the statistical definition of the variables with time and then combining them with the Boltzmann kinetic equation [2, 5, 7],

$$\begin{aligned} &\rho\frac{d(\mathbf{\Pi}/\rho)}{dt} + \nabla\cdot\boldsymbol{\psi}^{(\mathbf{\Pi})} + 2[\mathbf{\Pi}\cdot\nabla\mathbf{u}]^{(2)} + 2\,p[\nabla\mathbf{u}]^{(2)} = \mathbf{\Lambda}^{(\mathbf{\Pi})}, \\ &\rho\frac{d(\mathbf{Q}/\rho)}{dt} + \nabla\cdot\boldsymbol{\psi}^{(\mathbf{Q})} + \boldsymbol{\psi}^{(\mathbf{P})} : \nabla\mathbf{u} + \mathbf{Q}\cdot\nabla\mathbf{u} + \frac{d\mathbf{u}}{dt}\cdot\mathbf{\Pi} + \mathbf{\Pi}\cdot\nabla(C_pT) + p\nabla(C_pT) = \mathbf{\Lambda}^{(\mathbf{Q})}, \end{aligned} \tag{5}$$

Here, C_p is the heat capacity per mass at constant pressure. In the constitutive equations (5), $\boldsymbol{\psi}^{(\mathbf{\Pi},\mathbf{Q},\mathbf{P})}$ represent the open high-order terms of the viscous stress tensor, and the heat flux, respectively. $\mathbf{\Lambda}^{(\mathbf{\Pi},\mathbf{Q})}$ on the right-hand side of Eq. (5) represent the dissipation in the non-conserved quantities which is attributed to the collisional operator in the kinetic equation. At this point, it should be mentioned that the constitutive equations (5) are an exact consequence of the Boltzmann equation [2, 5, 7] and are thus capable of capturing the whole flow physics if they are provided with accurate closure on the open higher-order terms $\boldsymbol{\psi}^{(\mathbf{\Pi},\mathbf{Q},\mathbf{P})}$ and $\mathbf{\Lambda}^{(\mathbf{\Pi},\mathbf{Q})}$.

In the present work, we implement this observation with the key difference that instead of analytically deriving the accurate closure of these higher-order terms in the constitutive equations (5), we simply

employ the closed solution of DSMC in combination with DNN to reach a closed representation of these constitutive relations. Therefore, the current methodology does not suffer the so-called closure problem.

To attain accurate closure of the constitutive equations (5), these relations require DSMC data or a higher-order formulation consisting of nonlinear coupled functions f_{Π}, f_{Q} , which for direct implementation in the conservation laws can be expressed as,

$$\begin{aligned} \mathbf{\Pi}_{DSMC\ or\ Higher\text{-}order} &= f_{\Pi}\left(\mathbf{\Pi}_{NSF}, \mathbf{Q}_{NSF}\right), \\ \mathbf{Q}_{DSMC\ or\ Higher\text{-}order} &= f_{\mathrm{Q}}\left(\mathbf{\Pi}_{NSF}, \mathbf{Q}_{NSF}\right). \end{aligned} \tag{6}$$

It should be mentioned here that the first-order quantities such as $\mathbf{\Pi}_{NSF\,(DSMC)} = -2\mu(T_{DSMC})\left[\nabla \mathbf{u}_{DSMC}\right]^{(2)}$ were introduced as a bookkeeping role to efficiently construct the topology of DSMC constitutive relations to be coupled with the conservation laws (2). Therefore, introducing these quantities does not contaminate the DSMC constitutive data and does not affect the final solutions in principle.

On the other hand, the simplest *second-order* NCCR model that contains the essence of the nonlinearity and tight-coupling in the nonlinear coupled constitutive relations can be expressed as follows [1, 5, 7, 34, 35]:

$$\begin{aligned} \hat{\mathbf{\Pi}} q_{2nd\text{-}order}(c\hat{R}) &= \hat{\mathbf{\Pi}}_{NSF} + [\hat{\mathbf{\Pi}} \cdot \nabla \hat{\mathbf{u}}]^{(2)}, \\ \hat{\mathbf{Q}} q_{2nd\text{-}order}(c\hat{R}) &= \hat{\mathbf{Q}}_{NSF} + \hat{\mathbf{\Pi}} \cdot \hat{\mathbf{Q}}_{NSF}, \end{aligned} \tag{7}$$

where

$$q_{2nd-order}(c\hat{R}) = \frac{\sinh(c\hat{R})}{c\hat{R}},\ \hat{R} = \left[\hat{\mathbf{\Pi}} : \hat{\mathbf{\Pi}} + \hat{\mathbf{Q}} \cdot \hat{\mathbf{Q}}\right]^{1/2}.$$

Here *c* is the coefficient of gas power laws [1]. The following dimensionless and hat quantities have been applied:

$$
\begin{aligned}
&M = \frac{u_r}{\sqrt{\gamma R_g T_r}},\ \ \mathrm{Re} = \frac{\rho_r u_r L}{\mu_r},\ N_\delta = \frac{\gamma M^2}{\mathrm{Re}},\ \ \mathrm{Kn} = \sqrt{\frac{\pi}{2\gamma}}\frac{N_\delta}{M},\\
&\mathrm{Ec} = \frac{u_r^2}{C_{p_r} T_r},\ \ \mathrm{Pr} = \frac{c_{p_r}\mu_r}{k_r},\ \ \varepsilon = \frac{1}{\mathrm{EcPr}},\\
&\hat{\mathbf{\Pi}} \equiv \frac{N_\delta}{p}\mathbf{\Pi},\ \ \hat{\mathbf{Q}} \equiv \frac{N_\delta}{p}\frac{\mathbf{Q}}{\sqrt{T/(2\varepsilon)}},\\
&\hat{\mathbf{\Pi}}_{NSF} \equiv \frac{N_\delta(-2\mu[\nabla\mathbf{u}]^{(2)})}{p},\ \nabla\hat{\mathbf{u}} \equiv \frac{N_\delta(-2\mu\nabla\mathbf{u})}{p},\ \ \hat{\mathbf{Q}}_{NSF} \equiv \frac{N_\delta}{p}\frac{(-k\nabla T)}{\sqrt{T/(2\varepsilon)}}.
\end{aligned}
\tag{8}
$$

Here the subscript *r* represents the reference state and *L* denotes the characteristic length.

In traditional CFD solvers, where the majority of the solution techniques are based on the numerical solution of some PDE, to gain a theoretical understanding of physical phenomena (for example, Prandtl's boundary layer theory), one can analyze the relationship between the mathematical equations, their structure, and solution behavior.

In recent years, data-driven modeling has proven to be a practical tool in various fields of science and technology, capable of extracting essential physics from the data. Thus, in the current work, data-driven modeling will be employed for extracting the higher-order constitutive relations (as formulated in Eq. 6) from the DSMC solution data, and this model will serve as the constitutive relations to the conventional FVM solver of the conservation laws, which are fundamental laws of physics.

A. Shock wave structure problem

A stationary shock wave structure is a pure one-dimensional compressive gas flow that manifests as a sliver of a stationary gas flow region (order of mean free path) [46]. It forms between the supersonic upstream and the subsonic downstream. This flow is the most widely studied problem in gas dynamics [47-51], as the physical understanding of this flow has crucial technological implications.

The advantage of this flow (on top of being a one-dimensional case) is the absence of boundary conditions. Thus, the shock structure problem is an ideal case to test a new numerical algorithm, as the solution does not suffer from the contamination caused by the solid wall boundary condition.

The conservation laws that need to be solved to obtain the numerical solution for the shock structure problem are,

$$\frac{\partial}{\partial t}\begin{bmatrix}\rho\\ \rho u\\ \rho E\end{bmatrix}+\frac{\partial}{\partial x}\begin{bmatrix}\rho u\\ \rho uu+p+\Pi_{xx}\\ \left(\rho E+p+\Pi_{xx}\right)u+Q_x\end{bmatrix}=0\,. \tag{9}$$

To further emphasize the importance of the requirement for higher-order constitutive relations, the density distributions in the shock structure are compared in Fig. 1 for solutions obtained by NSF, NCCR, and DSMC. Differences in the numerical predictions of each solver result from the difference in the estimation of viscous shear stress and heat flux by the constitutive relations unique to each method.

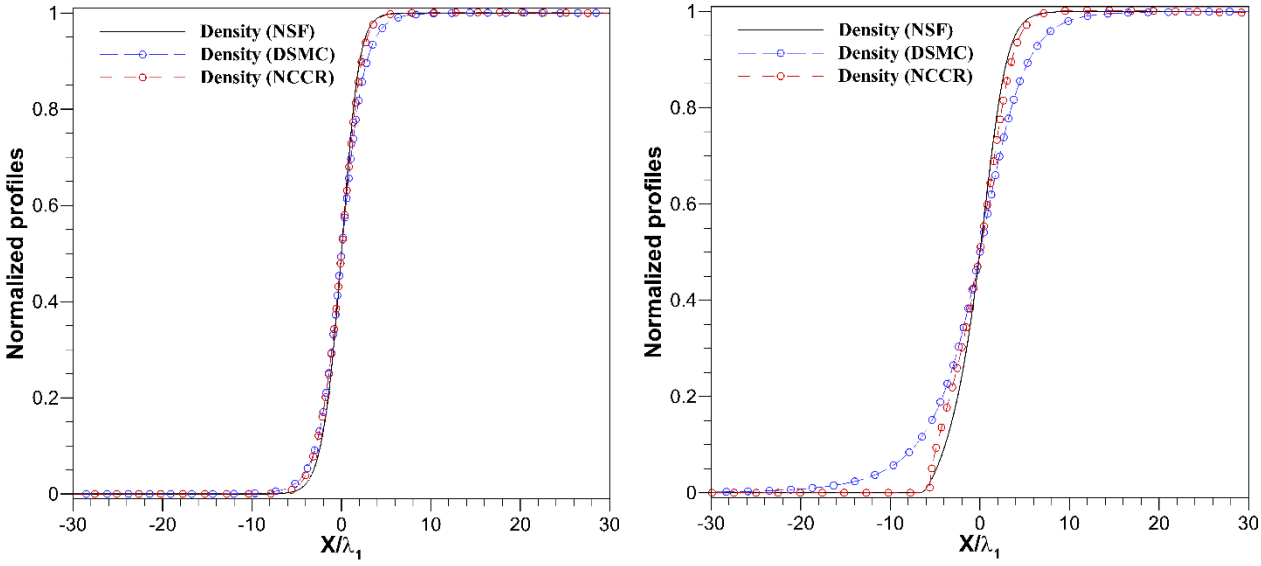

(a) M = 2 (b) M = 10

FIG. 1. Comparison of normalized density profiles predicted by NSF, NCCR, and DSMC for Mach numbers; (a) M = 2 and (b) M = 10.

Comparisons of the viscous stress and heat flux computed by the constitutive relations of each of these methods are presented in Figs. 2 and 3, respectively. Thus, the present work aims to develop data-driven models of constitutive relations that estimate the viscous stress and heat flux with accuracy equivalent to DSMC.

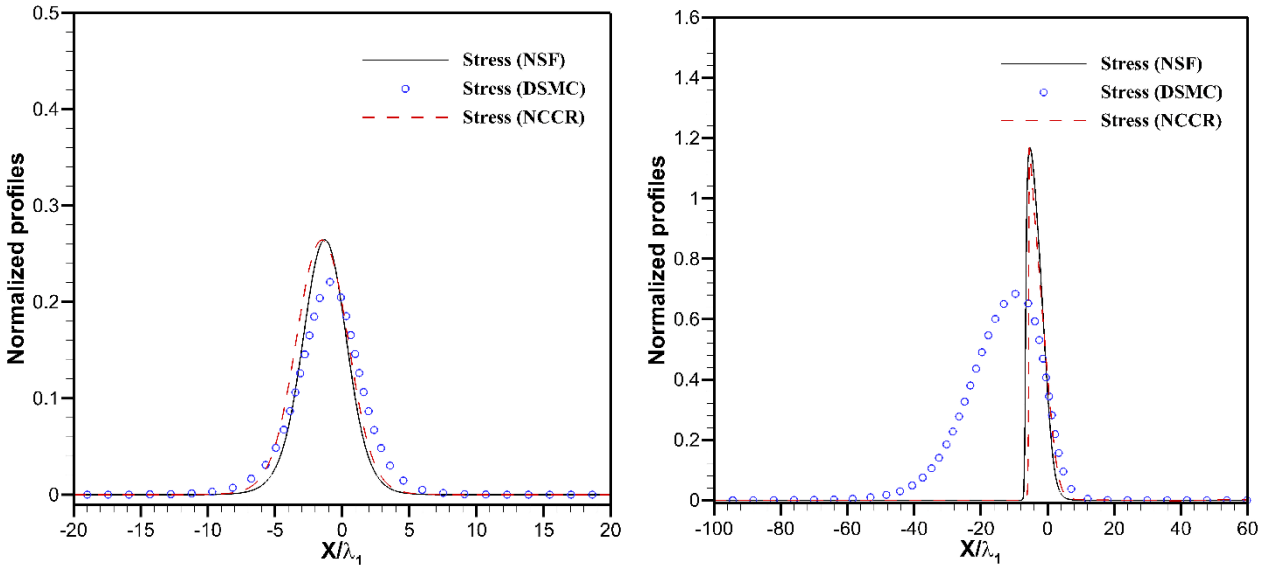

(a) M = 2 (b) M = 10

FIG. 2. Comparison of normalized viscous stress profiles predicted by NSF, NCCR, and DSMC for Mach numbers; (a) M = 2 and (b) M = 10.

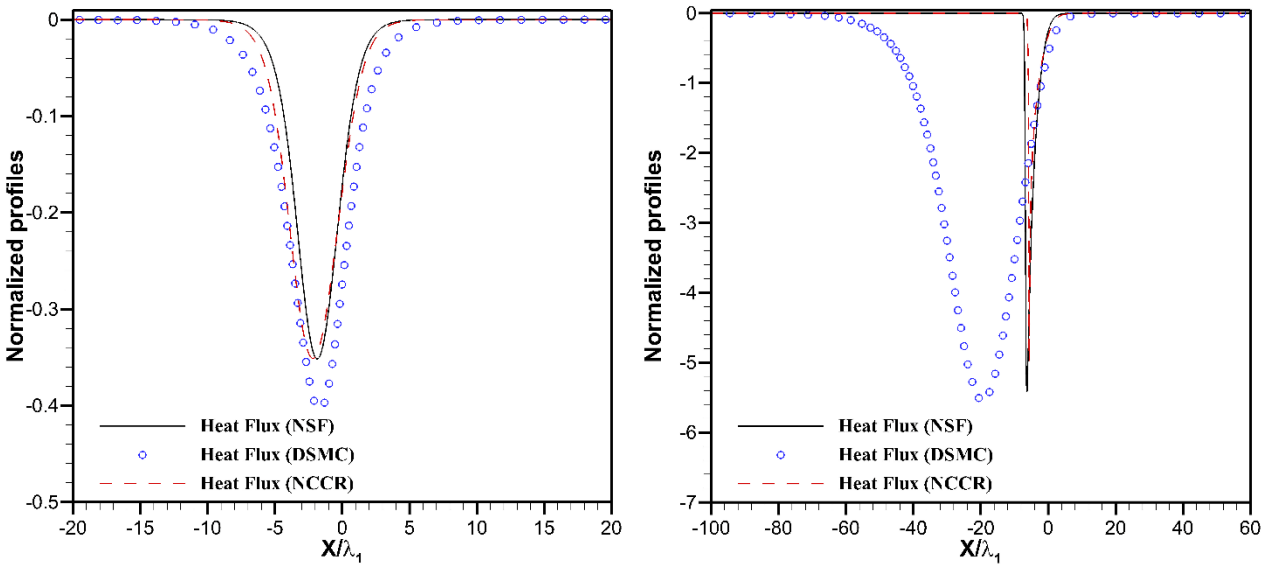

(a) M = 2 (b) M = 10

FIG. 3. Comparison of normalized heat flux profiles predicted by NSF, NCCR, and DSMC for Mach numbers; (a) M = 2 and (b) M = 10.

B. Computational methodology

The computational methodology consists of two parts. The first is the development of a DNN model, which contains the extracted higher-order constitutive relationships, and the second is the development of an FVM solver capable of solving the conservation laws in conjunction with these constitutive relationships. The FVM solver developed for the present study is based on the second-order monotonic upwind scheme for conservation laws (MUSCL) [52] with a min-mod limiter, Harten-Lax-van Leer-Contact (HLLC) flux solver [53] for the convective terms, and a central difference scheme for the calculation of viscous terms. The time integration of the set of conservation laws is achieved via the explicit Euler method.

The details of the algorithm employed to develop the present DNN model for DSMC or a solution methodology that encompasses higher-order constitutive relations can be summarized as follows:

Step 1. Generation of data.

For the current study, this is achieved with numerical solutions of the flow problem for a range of critical parameters (Mach Numbers in the case of the shock structure problem) using DSMC or a solution methodology that encompasses higher-order constitutive relations. This step provides the solution for DSMC or higher-order stress and heat flux ($\mathbf{\Pi}_{DSMC\ or\ Higher\text{-}order}, \mathbf{Q}_{DSMC\ or\ Higher\text{-}order}$).

Step 2. Computing the following values from data obtained in Step 1.

a) NSF linear viscous stress ($\mathbf{\Pi}_{NSF}$) is calculated using the velocity information obtained in Step 1. The viscosity (μ) is assumed to be a function of temperature and is calculated using the relation,

$$\mu = \mu_{ref} \left(T / T_{ref} \right)^{\omega} \ . \tag{10}$$

Here μ_{ref} is the reference viscosity, T_{ref} the reference temperature, and ω the coefficient of viscosity. In the current work, ω is '1' (Maxwellian molecule), μ_{ref} is 2.117×10^{-5} kg/m·s, and T_{ref} is 273.15 K.

b) NSF linear heat flux ($\mathbf{Q}_{NSF}$) is calculated using the temperature information obtained in Step 1. The thermal conductivity is estimated using the following relation (Pr=0.75),

$$k = \mu C_p / \mathrm{Pr} \ . \tag{11}$$

Step 3. Training the DNN model of constitutive relations.

The input for this modeling is the $\mathbf{\Pi}_{NSF}$ (explained in Step 2a) and $\mathbf{Q}_{NSF}$ (explained in Step 2b) and the output for this model is $\mathbf{\Pi}_{DSMC\ or\ Higher\text{-}order}$ and $\mathbf{Q}_{DSMC\ or\ Higher\text{-}order}$. The DNN model maps the linear viscous stress and heat flux into the DSMC or higher-order viscous stress and heat flux. Figure 4 presents the pictorial representation of how the topology on the DNN model looks like.

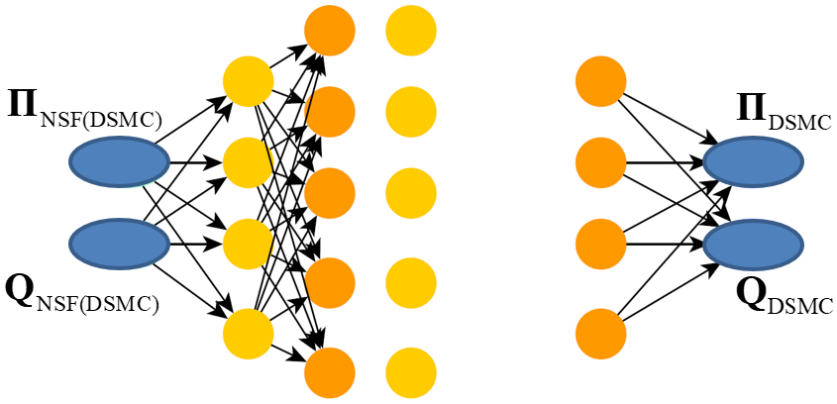

FIG. 4. Topology on the DNN model of constitutive relations.

When developing a DNN model, in addition to the choice of the input and output parameters, various other DNN-related parameters require careful selection. These parameters include the number of hidden layers, number of neurons in each layer, epoch, learning rate, batch size, type of activation function, and optimizer function. The optimizer and the activation function are chosen as '**adam**' and

'**relu**', respectively, in the present work. Since the numeric values of the rest of the parameters are dependent upon the quality and size of the data, these parametric values are problem-dependent and were chosen accordingly (i.e., the aim was to avoid over-fitting).

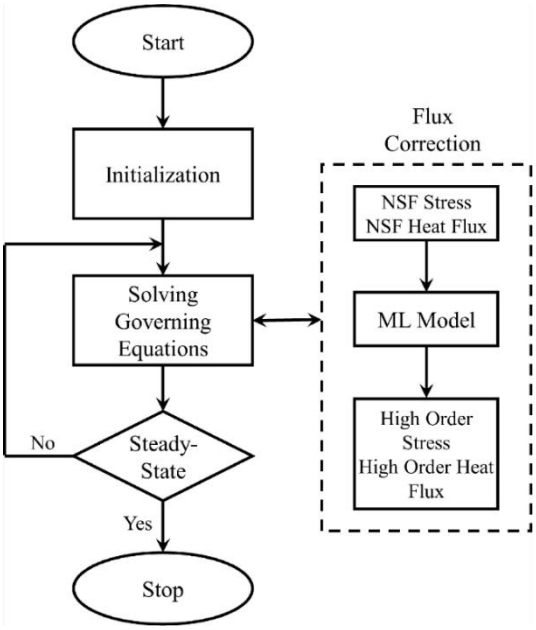

FIG. 5. Flowchart of the algorithm employed in the FVM-ML solver.

The next step is implementing the DNN model within a conventional FVM framework which is achieved by the following algorithm:

Step I. Estimating the NSF flux at the cell interface using the methodology explained previously in Step 2. Here, the macroscopic properties used for calculation are the initial values for that iteration.

Step II. The estimated value of NSF flux is normalized using the methodology given in (8) and explained in detail by Myong [1, 34, 35]. These normalized values are the input to the DNN model, and the corrected flux, i.e., the output from the DNN model, is communicated back to the FVM solver.

Step III. The solution for the current iteration proceeds by employing these corrected fluxes (communicated by the DNN model).

The FVM-ML solver keeps iterating until the solution converges. The progress of the simulation towards convergence is monitored by calculating the L1 error in macroscopic properties density, velocity, and temperature by employing

$$\text{L1 } error = \frac{1}{N_{cell}} \sum_{i=1}^{N_{cell}} abs\left(\phi_i^{t+1} - \phi_i^{t}\right). \tag{12}$$

Here ϕ represents density, temperature, and velocity, and N_{cell} is the mesh number. The solution is assumed to achieve convergence when the value of the L1 error is $\leq 10^{-6}$ for all the monitored macroscopic properties. For more clarity, Fig. 5 presents the flowchart of the algorithm implemented in the FVM-ML solver.

C. Verification of the FVM-NCCR-ML strategy

Before combining the FVM-ML algorithm with DSMC, this methodology is tested by replicating the FVM-NCCR solutions for the shock structure problem. The upstream pressure (p_1) and temperature (T_1) chosen for this study are 6.6595 Pa and 300 K, respectively. Based on the upstream conditions and the flow Mach number (M_1), the remaining required macroscopic properties are calculated employing the Rankine-Hugonoit relations [46] that are as follows,

$$\begin{aligned}
&\frac{p_2}{p_1} = 1 + \frac{2\gamma}{\gamma+1}\left(M_1^2 - 1\right), \\
&M_2^2 = \frac{1 + \left[(\gamma-1)/2\right] M_1^2}{\gamma M_1^2 - (\gamma-1)/2}, \\
&\frac{T_2}{T_1} = \left[1 + \frac{2\gamma}{(\gamma+1)}\left(M_1^2 - 1\right)\right]\left[\frac{2 + (\gamma-1) M_1^2}{(\gamma+1) M_1^2}\right].
\end{aligned} \tag{13}$$

In the equations above, subscript '1' indicates the upstream conditions, and the subscript '2' indicates the downstream conditions. The specific heat value (γ) is 1.667 (since the working gas is a monatomic gas). Thus, based on the upstream conditions, the mean free path of the current study is 6.564×10^{-4} m, and the simulated domain extends from [-30.0, 30.0] times the upstream mean free path (containing 500 cells).

The initial discontinuity is placed at the center of the domain. The data for developing the DNN model is generated (from the in-house NCCR solver) for Mach numbers 2, 4, 6, 8, and 10.

Both the in-house one-dimensional FVM-NCCR-ML and FVM-NCCR are based on the methodology explained in Section II.B. The transport coefficients, i.e., viscosity and thermal conductivity, are calculated employing the temperature-dependent power laws as defined in Eqns. (10) and (11) respectively. The value of the coefficient of the gas power law ω is '1.0', the reference temperature $T_{ref}\left(=273.15\ \mathrm{K}\right)$, the reference viscosity (μ_{ref}) is 2.117×10^{-5} Pa·s, and the assumed Prandtl number (Pr = 0.75).

Before carrying out the FVM-NCCR-ML simulations of conserved (density, velocity, and temperature) and non-conserved (viscous stress and heat flux) properties using the developed DNN model, the distribution of non-conserved properties estimated by this model is compared with the one predicted by NCCR. Figures 6 and 7 compare two Mach number cases, 2 and 10, respectively. From these figures, one can observe that the DNN model predicts the overlapping results.

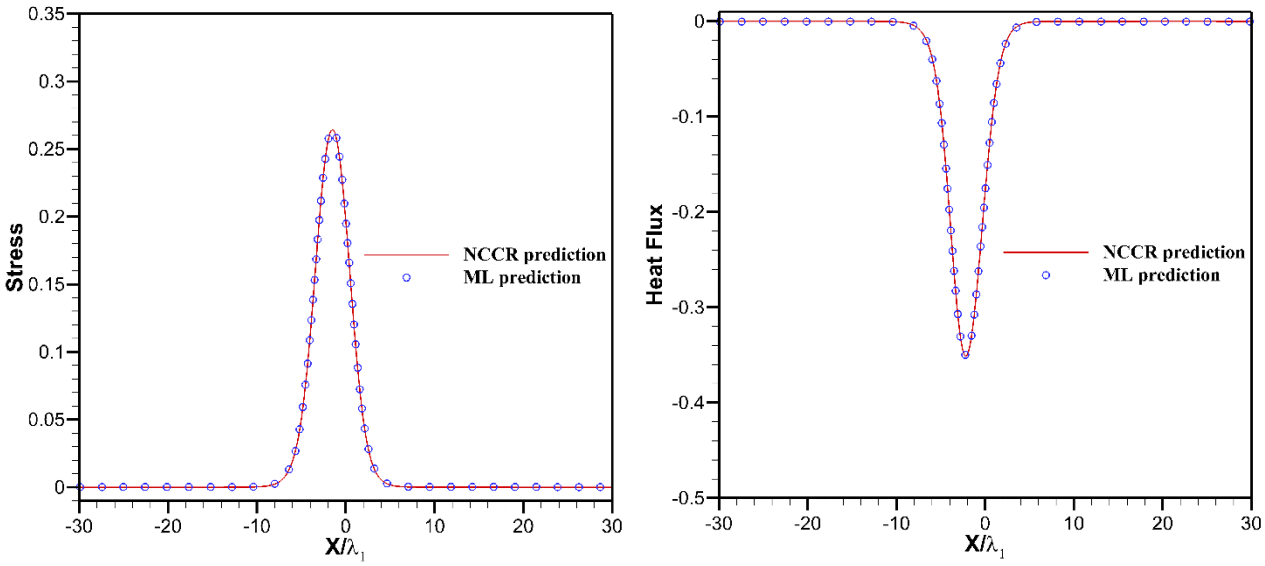

(a) Viscous stress (b) Heat flux

FIG. 6. Comparison of non-conserved viscous stress and heat flux profiles predicted by the DNN model

with the actual results from the NCCR solver for the Mach 2 case; (a) viscous stress and (b) heat flux.

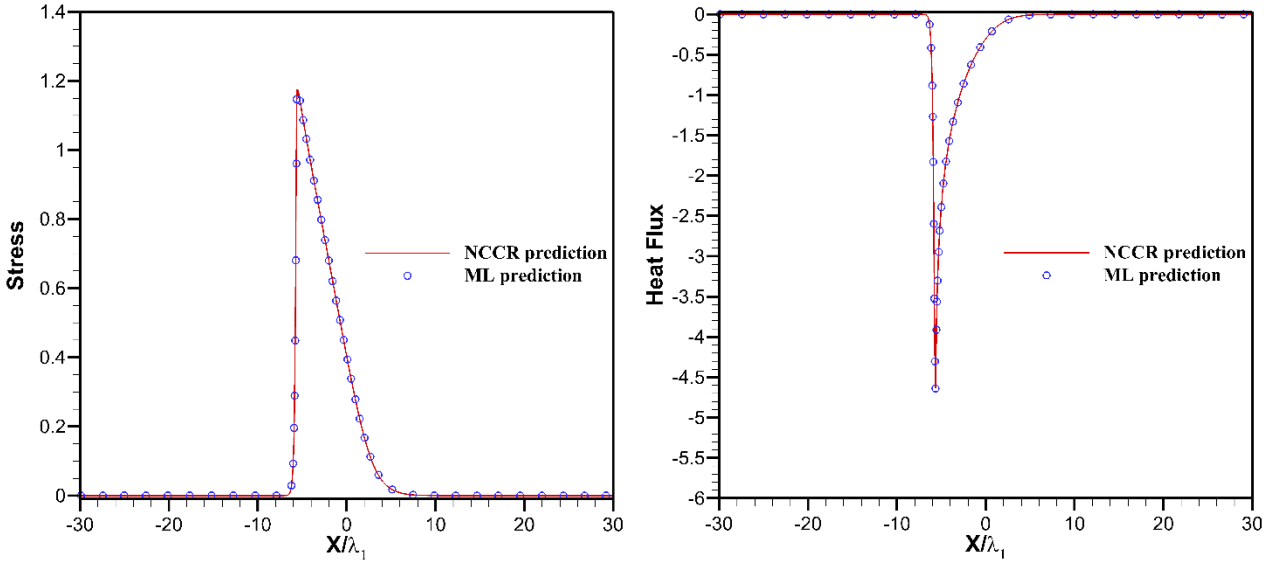

(a) Viscous stress (b) Heat flux

FIG. 7. Comparison of non-conserved viscous stress and heat flux profiles predicted by the DNN model with the actual results from the NCCR solver for the Mach 10 case; (a) viscous stress and (b) heat flux.

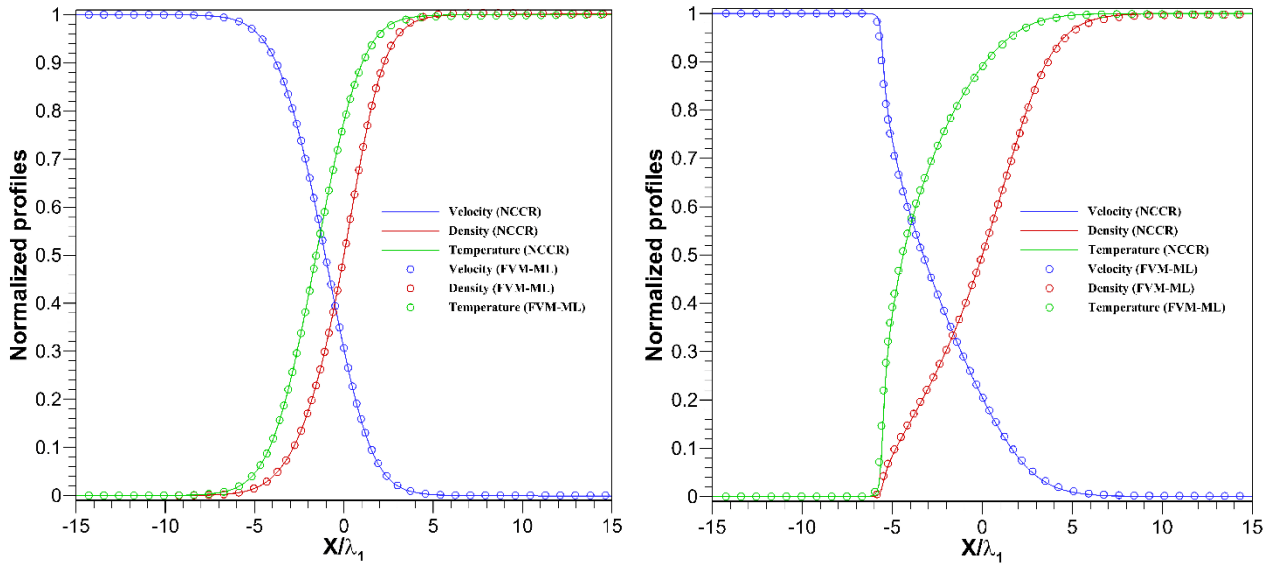

(a) M = 2 (b) M = 10

FIG. 8. Comparison of normalized conserved macroscopic properties (density, velocity, and temperature)

of the FVM-NCCR-ML and FVM-NCCR solutions for Mach numbers; (a) M = 2 and (b) M = 10.

The next test compares conserved macroscopic properties (density, velocity, and temperature) of the FVM-NCCR-ML and FVM-NCCR solutions for the Mach numbers 2, 4, 6, 8, and 10. The Courant number for all the simulations is 0.45, and the time-step is calculated based on the correlations presented in [34]. For brevity, only the results for Mach numbers 2 and 10 are presented in Figs. 8a and 8b, respectively. The conserved macroscopic properties are normalized employing the following relation,

$$\Phi_{norm} = \frac{\Phi_{cell} - \Phi_1}{\Phi_2 - \Phi_1}, \text{ where } \Phi \text{ is either } \rho \text{ or } T, \tag{14}$$

$$V_{norm} = \frac{V_{cell} - V_2}{V_1 - V_2} \ . \tag{15}$$

The results for all the cases show excellent agreement in FVM-NCCR-ML and FVM-NCCR solutions.

When comparing the computational cost, that of the FVM-NCCR-ML solver ranges from approximately 1.1 to 1.2 times the standard FVM-NCCR solver. The cost increases as the shock Mach number increases with approximately 1.2 times being the maximum at Mach number 10.

III. DSMC SOLUTIONS USING THE FVM-DSMC-ML SOLVER

The current section presents the FVM-DSMC-ML solver that aims to provide the DSMC solution for the shock structure problem. For the first case, a machine learning model of the constitutive relations is developed individually for each Mach number. The second case tests a practically implementable case, i.e., developing a single DNN model of the constitutive relations for all the Mach numbers ranging from 2 to 10.

A. DNN constitutive relation model for individual Mach numbers

This section presents the case wherein the DNN model from DSMC data is trained for each Mach number individually. The methodology implemented here, i.e., developing different DNN models for each Mach number, does seem impractical but can be construed as a confidence-building exercise.

Thus, in this study, first, the data for the shock structure problem is generated for Mach numbers 2, 4, 6, 8, and 10 employing the in-house MPI parallelized DSMC solver and then, utilizing the algorithm explained in Section II.B, a DNN model of constitutive relations is trained for each Mach number. Next, simulations are carried out for the shock structure problem using the FVM-DSMC-ML solver (the solver methodology is explained in Section II.B), and these results are compared with the DSMC solution.

In the current study, the simulations are carried out with a monatomic gas (molecular diameter 4.618×10^{-10} m and molecular mass 6.64×10^{-26} kg) as the working gas. The value of the coefficient of viscosity (ω) for all the simulations is set to '1.0' (Maxwellian molecule) for the sake of simplicity. Other values of the viscosity coefficient can be treated without any change. The upstream conditions, i.e., density and temperature for all the cases, are 1.068×10^{-4} kg/m^3 and 273.15 K, respectively. The upstream mean free path (λ_1) is 6.564×10^{-4} m (the cell width is 1/50th of the upstream mean-free path), and the time-step for the DSMC simulations is 1/100th of the mean collision time (τ) based on the upstream conditions. The weight ratio (i.e. the number of real molecules a single DSMC particle represents) is 5.0×10^{13} and the domain extends from [-150.0,150.0] times the upstream mean free path.

The initial discontinuity is placed at the center and the remaining upstream and downstream conditions are calculated using the Rankine-Hugonoit relations presented in Eq. (13). In the current in-house DSMC solver the sampling cells are intentionally kept the same as the collision cells to achieve a better resolution of the solution which is deemed as a requirement for proper DNN modeling.

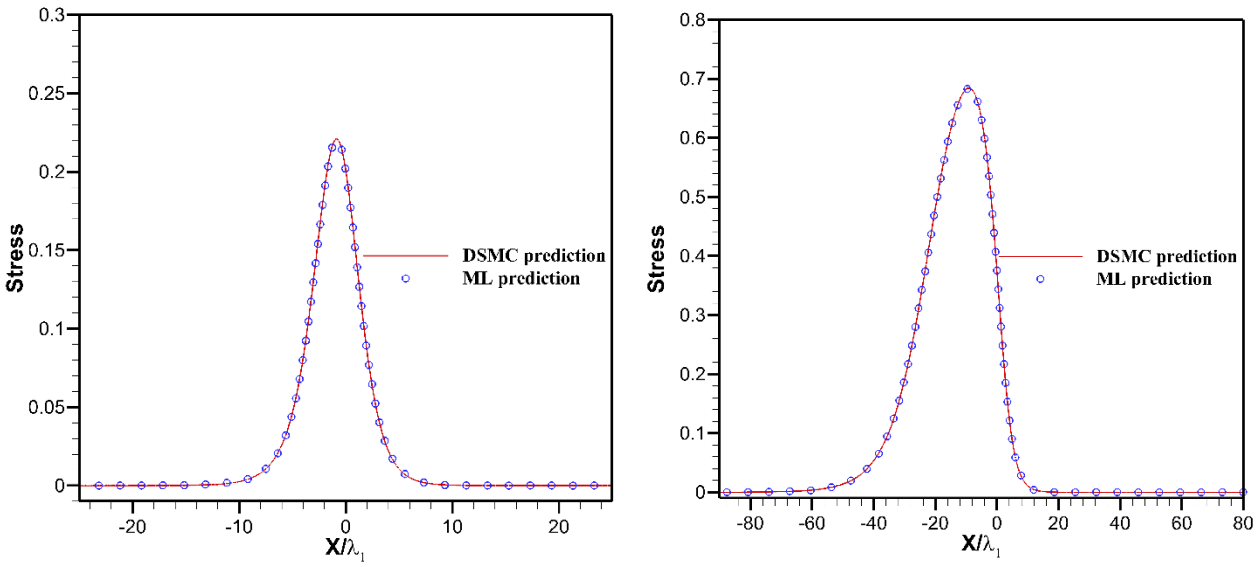

(a) M = 2 (b) M = 10

FIG. 9. Comparison of viscous stress predicted by the DNN model developed using the data of a single Mach number with the actual results from the DSMC for the Mach numbers; (a) 2 and (b) 10.

The DSMC solution carries out sampling until the DSMC stress ($\mathbf{\Pi}_{DSMC}$) and heat flux ($\mathbf{Q}_{DSMC}$) predictions are smooth (requiring ≈ 1 million samples), but even after these many samples, the calculated values of DSMC linear stress ($\mathbf{\Pi}_{NSF}$) and heat flux ($\mathbf{Q}_{NSF}$) remain noisy. This noise results from the solution methodology employed in DSMC, which is probabilistic in nature. To achieve a smooth solution for linear stress and heat flux, these predictions from DSMC are filtered. The algorithm employed to achieve a filtered solution can be summarized as follows:

i. This process treats the predictions of linear viscous stress and heat flux from the DSMC as a signal that is a function of space and first calculates the fast Fourier transform of the signal, which provides the signal frequency vs amplitude distribution. This distribution provides the cut-off frequency, i.e., the frequency beyond which the amplitude of the stress and heat flux solution is negligible.

ii. In the next step, based on this frequency, the data is filtered employing a low pass filter. The low pass filter employed in the current study is the Butterworth filter, and the order of filtering is '2'.

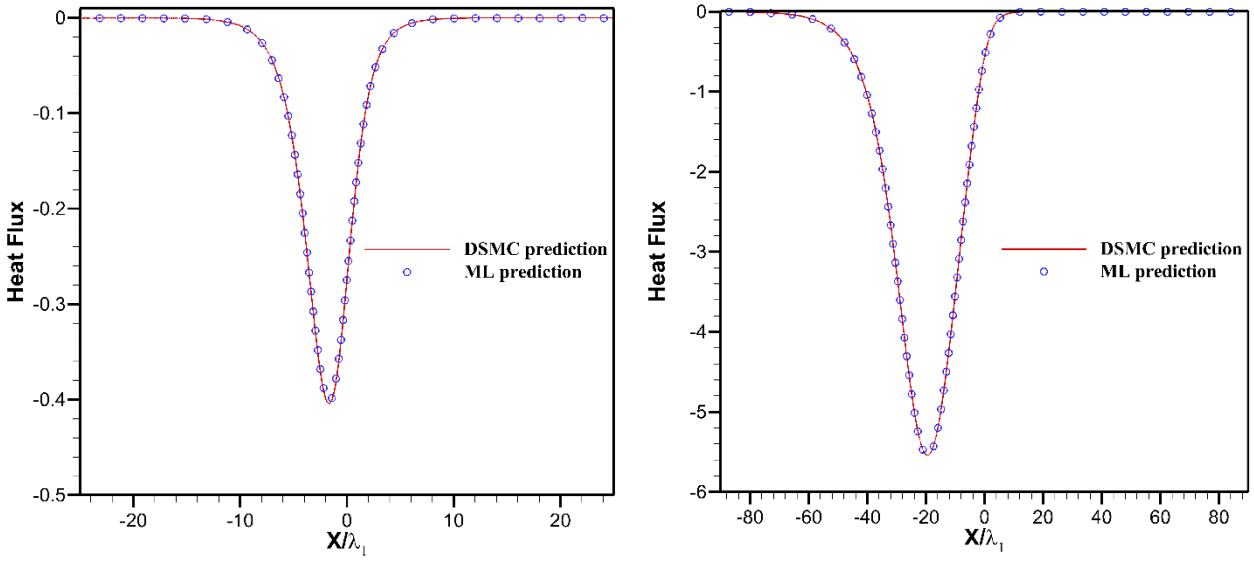

(a) M = 2 (b) M = 10

FIG. 10. Comparison of heat flux predicted by the DNN model developed using the data of a single Mach number with the actual results from the DSMC for the Mach numbers; (a) 2 and (b) 10.

As carried out in Section II.C, first, the estimations of viscous stress and heat flux by the DNN model are compared with its counterpart predicted by DSMC for all the Mach numbers. For succinctness, Figs. 9 and 10 present this comparison for only two Mach numbers, 2 and 10. From the comparison, one can observe that the estimations from the DNN model overlap with the DSMC values.

To further validate the solution algorithm, the shock structure problem is simulated using the FVM-DSMC-ML solver (which employs the DNN model trained for the respective Mach number), and the results from these simulations are compared with the DSMC solution for similar conditions. The Courant number, convergence monitoring, and time-step calculation follow a similar protocol as mentioned in Section II.C.

Figures 11 (a) and (b) compare the normalized profiles of density, temperature, and velocity predicted by the FVM-DSMC-ML and DSMC solver for two Mach numbers, 2 and 10, respectively. From these figures, one can perceive that the simulation results from both the solvers overlap.

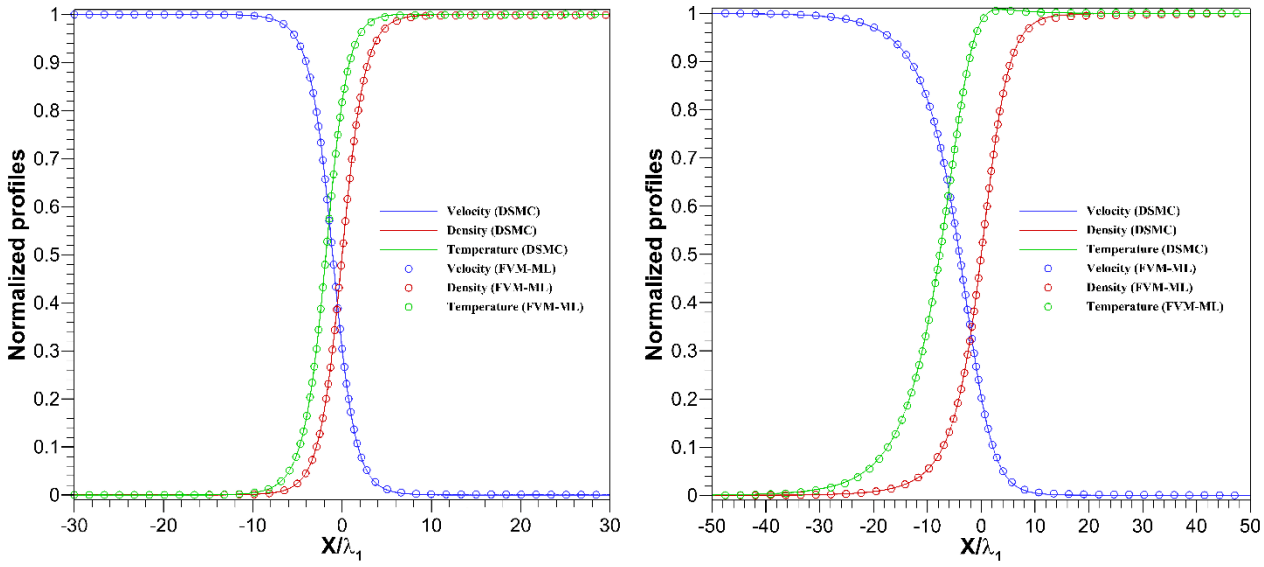

(a) M = 2 (b) M = 10

FIG. 11. Comparison of normalized conserved macroscopic properties (density, velocity, and temperature) of the FVM-DSMC-ML and DSMC solutions for Mach numbers; (a) 2 and (b) 10. The DNN model employed here is trained individually for each Mach number.

When comparing the computational cost, a single DSMC simulation (which is simulated by the in-house Fortran solver) took approximately 200 hours on 26 processors, while the FVM-DSMC-ML solver (which is developed in-house in Python) took only about 20 hours on a single processor (which is 1.5 times higher than that of the FVM-NSF solver). As far as the computational cost of DNN modeling is concerned, the model training took approximately 15-20 minutes on a single processor. Thus, the new method provides a massive reduction in computational cost while preserving solution accuracy.

B. DNN constitutive relation model for all the Mach numbers

We confirmed in the previous sections that the present numerical algorithm performs well if tested for a Mach number whose DSMC data is a part of DNN model training. However, from a practical perspective, the model of constitutive relations should be able to predict the correct solution for a wide range of Mach numbers. Here we develop a single DNN model using the DSMC data for Mach numbers 2, 3, 4, 5, 6, 7, 8, 9, and 10 and then employ this DNN model in the FVM-DSMC-ML solver to predict the results for other Mach numbers *whose data were not employed in training the DNN model*, i.e., 2.5, 4.5, 6.5, and 8.5.

The simulation parameters, i.e., gas properties and initial conditions for the current case, are similar to the ones chosen in the previous section. The DNN model uses 70% of the DSMC data for training and employs the remaining data for validation. The root mean square loss observed as the training of the DNN model progresses is presented in Fig. 12.

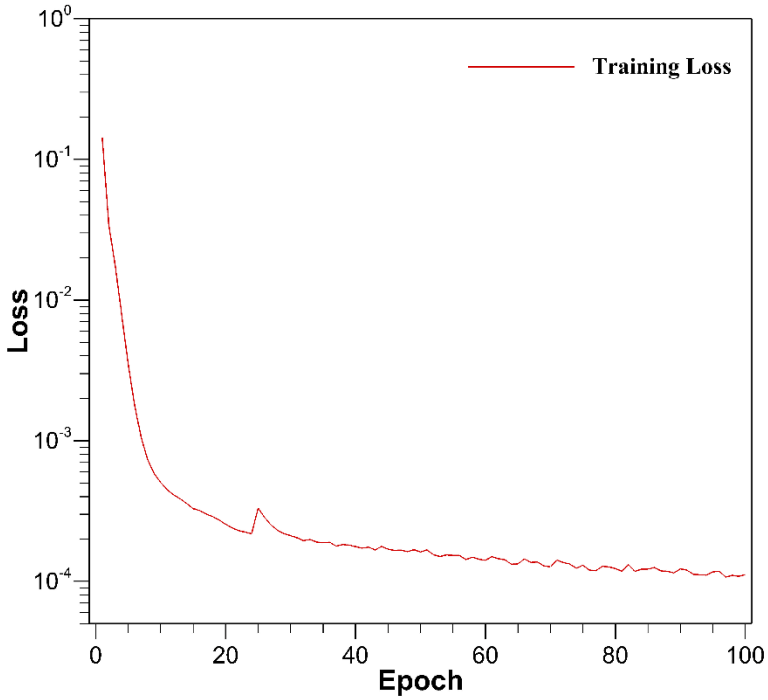

FIG. 12. Progress of root mean square loss in the DNN modeling.

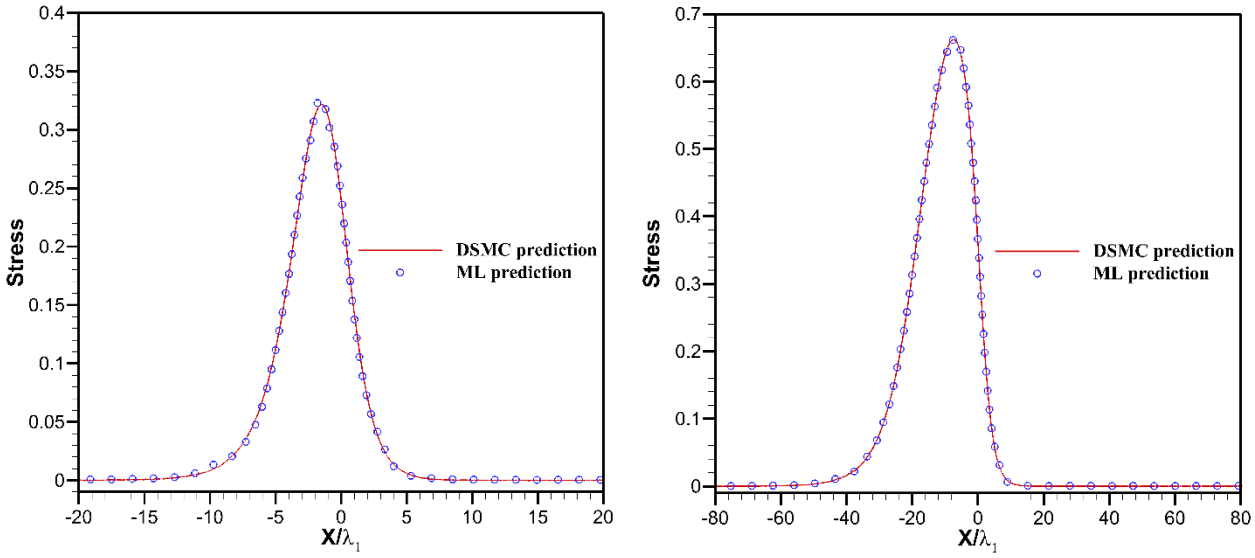

(a) M = 2.5 (b) M = 8.5

FIG. 13. Comparison of viscous stress predicted by the DNN model developed using the data for Mach numbers 2, 3, 4, 5, 6, 7, 8, 9, and 10 with the actual results from the DSMC for the Mach numbers; (a) 2.5 and (b) 8.5.

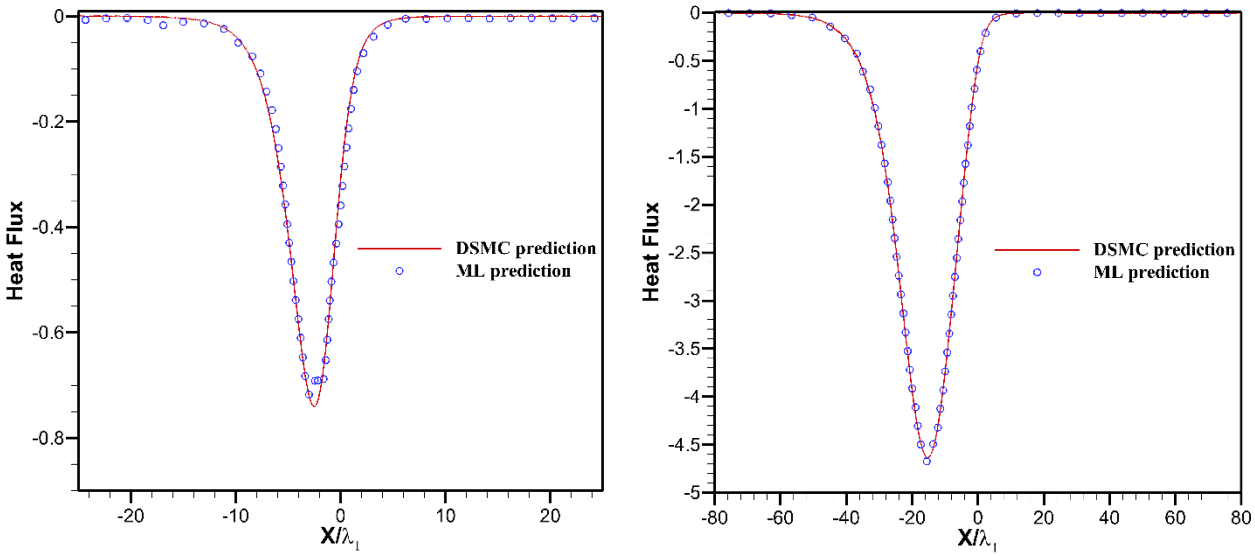

(a) M = 2.5 (b) M = 8.5

FIG. 14. Comparison of heat flux predicted by the DNN model developed using the data of Mach numbers 2, 3, 4, 5, 6, 7, 8, 9, and 10 with the actual results from the DSMC for the Mach numbers; (a) 2.5 and (b) 8.5.

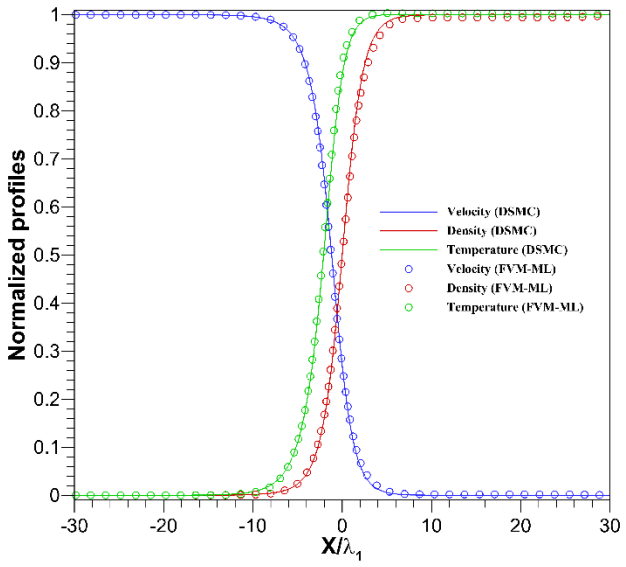

(a) M = 2.5

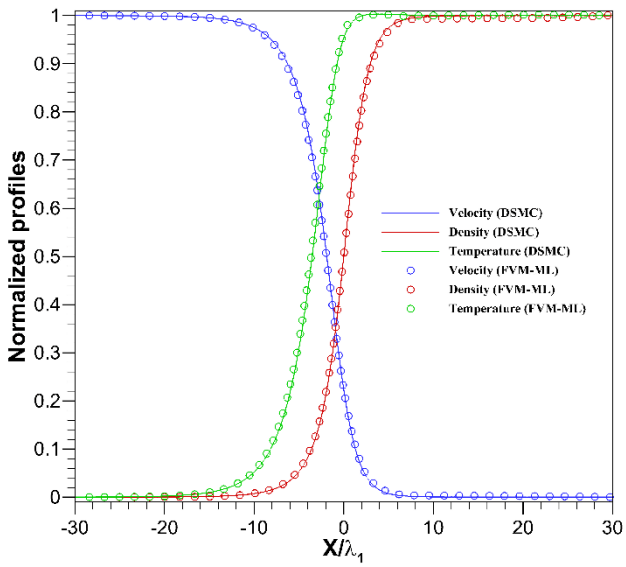

(b) M = 4.5

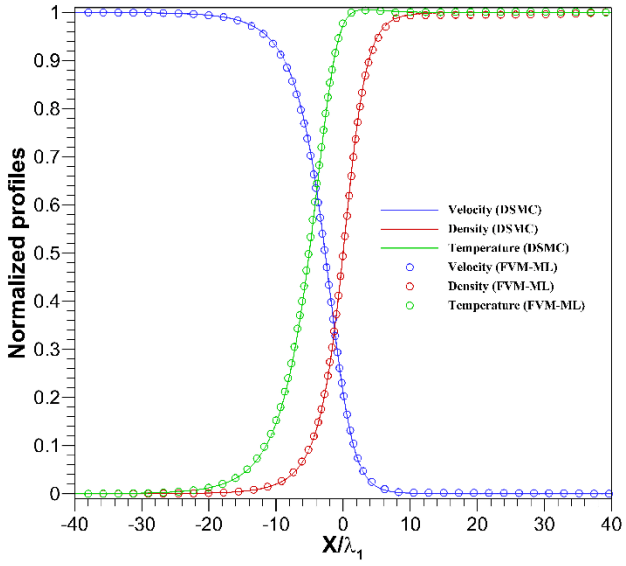

(c) M = 6.5

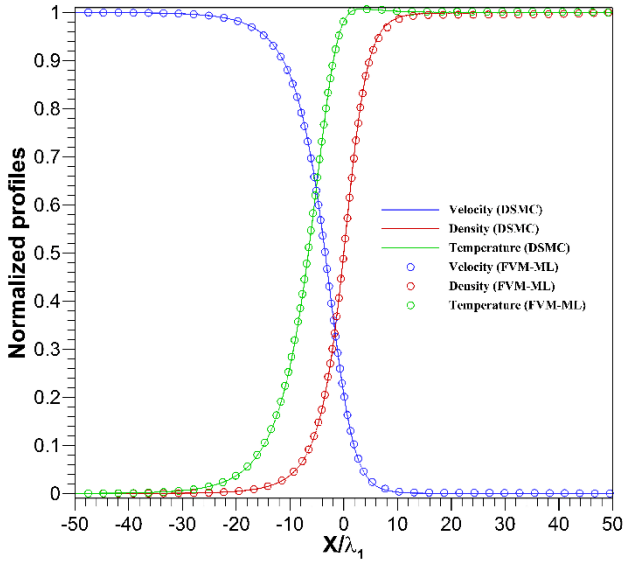

(d) M = 8.5

FIG. 15. Comparison of normalized conserved macroscopic properties (density, velocity, and temperature) of the FVM-DSMC-ML and DSMC solutions for Mach numbers; (a) 2.5, (b) 4.5, (c) 6.5, and (d) 8.5. The DNN model employed here is trained using data from Mach numbers 2, 3, 4, 5, 6, 7, 8, 9, 10.

Figures 13 and 14 compare non-conserved viscous stress and heat flux profiles provided by the DNN model developed using the DSMC data. From these figures, one can observe that the DNN model predicts the correct thickness of the viscous stress and heat flux profiles for all the Mach numbers.

The comparison of normalized conserved density, temperature, and velocity profiles predicted by the FVM-DSMC-ML and DSMC solutions are presented in Fig. 15. As with the previous individual Mach numbers, the simulation results show almost perfect agreement between the FVM-DSMC-ML and DSMC solutions. Likewise, the FVM-DSMC-ML solver took about 1.5 times more than the FVM-NSF solver (mainly due to the reduced time-step), showing that it is possible to significantly reduce computational cost while maintaining accuracy.

C. Topology of the DSMC constitutive relations

Topology is an important mathematical concept for understanding the properties of a system that are preserved under continuous change. The study of the topological aspects of the dynamics of fluids has been very instructive for describing fluid flows with complicated physics. One of the central ideas in topology is that objects can be treated in their own right, and knowledge of objects is independent of how they are embedded in spatial space. Topological representations in fluid dynamics may be categorized into several groups, including vortex and helicity, stability in a dynamical system, phase transition, and constitutive relations. For example, the topology of vortex and helicity provides a fundamental knowledge of the propensity of flows to form vortices or coherent structures in classical fluids [54, 55].

One of the main goals of this study is to develop the DNN-based constitutive relations from the DSMC data and obtain a better understanding of the DSMC topology so that it may provide confidence in the DNN-based DSMC constitutive relations. This is achieved by comparing the DNN-based DSMC topology for the case of untrained Mach numbers with the original DSMC topology for the training set.

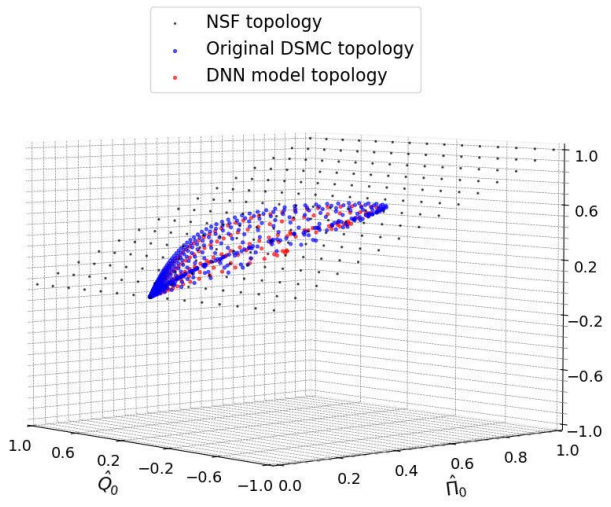

(a) 3D topology of viscous stress $\hat{\Pi}$

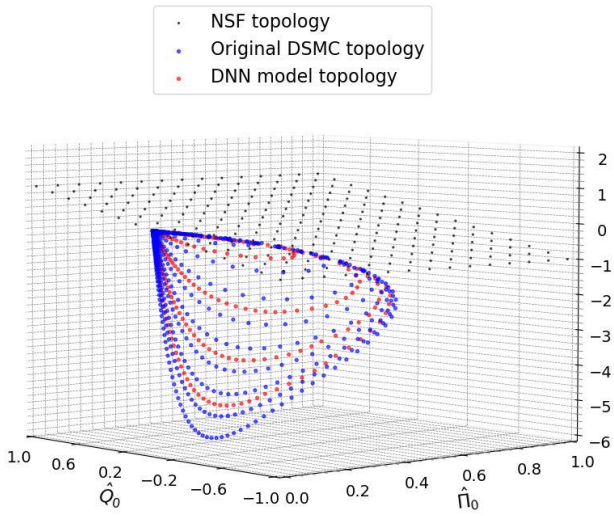

(b) 3D topology of heat flux $\hat{Q}$

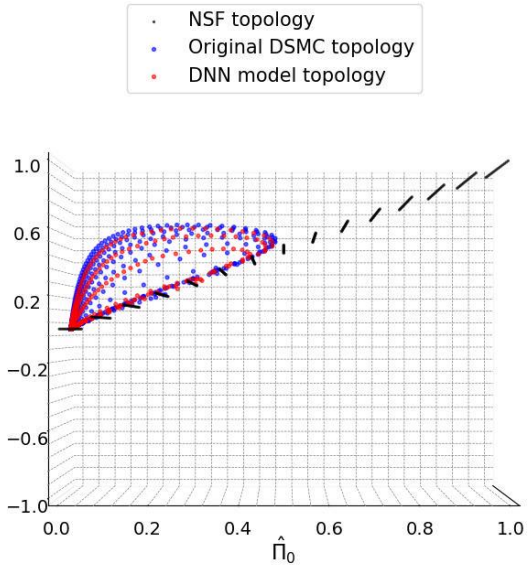

(c) 2D projection of topology of viscous stress $\hat{\Pi}$

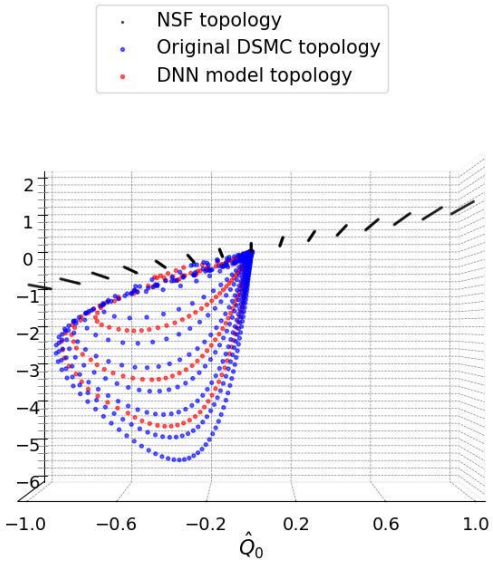

(d) 2D projection of topology of heat flux $\hat{Q}$

FIG. 16. Comparison of topologies of the DSMC constitutive relations and the DNN-based model; (a) 3D topology of viscous stress, (b) 3D topology of heat flux, (c) 2D projection of viscous stress topology on ($\hat{\Pi}_0$, $\hat{\Pi}$), and (d) 2D projection of heat flux topology on ($\hat{Q}_0$ and $\hat{Q}$).

Figure 16 presents three-dimensional topologies (original DSMC, DNN-based DSMC model, and NSF) for shock structure solutions, confined to the compressive flow regime with positive viscous stress and

negative heat flux. We believe these topologies to be new. The *x*, *y*, and *z*-axes in Figs. 16 (a) and (b) represent the normalized quantities ($\hat{\Pi}_0$, $\hat{Q}_0$, $\hat{\Pi}$) and ($\hat{\Pi}_0$, $\hat{Q}_0$, $\hat{Q}$), respectively. The blue-colored symbols represent the topology of the original DSMC data (for the Mach numbers whose data is used to train the DNN model in Section III.B) and the red-colored symbols represent the DNN-based DSMC topology for the intermediate Mach numbers, i.e., whose data was not included in the training of the DNN model. Figures 16 (c) and (d) present a two-dimensional projection of viscous stress topology on ($\hat{\Pi}_0$, $\hat{\Pi}$) and a two-dimensional projection of heat flux topology on ($\hat{Q}_0$, $\hat{Q}$).

The NSF topology (black-colored symbols) to the driving (viscous stress and thermal) forces is linear and has uncoupled viscous stress and thermal components. The viscous stress is a function of the viscous stress force but is independent of the thermal force. Likewise, the heat flux is a function of the thermal force but is independent of the viscous stress force.

On the other hand, the DSMC and DNN-based DSMC topologies become highly nonlinear when the flows are away from the LTE (local thermal equilibrium; origin in the figures). In addition, the topologies become strongly coupled to the viscous stress and thermal components, as evidenced by the curved surface in the thermal force direction for a specified value of viscous stress force. The viscous stress varies nonlinearly for the thermal force, although it is influenced more by the viscous stress force. Interestingly, though the topologies are highly nonlinear, they are smooth and neither overlap nor cross themselves. Furthermore, in most regimes, the values of viscous stress and heat flux in DSMC and DNN-based DSMC topologies are larger than those of NSF topology. This difference is responsible for different shock structure profiles observed in DSMC and NSF solutions, even though both DSMC and NSF obey the same conservation laws. Interestingly, all these characteristics were also observed in the case of the NCCR topology [55, Subsections III.B and IV.C].

IV. CONCLUDING REMARKS

The ultimate goal of this study is to build compact constitutive relations in advance by applying DNN-ML algorithms to available DSMC solution data and to combine them with conventional CFD codes such as FVM or DG for conservation laws to develop a third method (after PDE- and pure particle-based methods) for rarefied and microscale gas flows. In this context, DNN-ML models play the role of constructing constitutive relations in a multi-variable space for the elementary flows that will form the basis of all flow situations, replacing the traditional technique of deriving simple constitutive relations using experimental data or empirical methods.

Therefore, in principle, in addition to DSMC covered in this study, the present idea can be applied to molecular dynamics (MD) and gas kinetic solvers (GKS) in which explicit forms of PDEs for constitutive relations are not available. In such cases, it becomes possible to develop various solvers such as FVM-MD-ML and FVM-GKS-ML.

As a first step, we considered the one-dimensional shock wave internal structure problem, which is the most studied problem of non-equilibrium gas flow, and then developed a single DNN model using the DSMC solution data and the associated FVM-DSMC-ML solver that can provide solutions for arbitrary Mach numbers with the computing time comparable to that of the FVM-NSF Solver. The simulation results showed almost perfect agreement between the FVM-DSMC-ML and DSMC solutions for the conserved variables. We also constructed the topology of DSMC constitutive relations for the first time, which allowed us to study how the DSMC topology deviates from the NSF topology when the flow is away from local thermal equilibrium.

The present deep neural network-based FVM-DSMC-ML solver has been presented as an innovative method with great potential, but many challenging problems must be overcome to become a robust method suitable for solving real-world problems of scientific and technical interests.

First, in addition to the compressive flow branch of the topology of constitutive relations covered in this study, additional ML models must be developed for other flow branches such as the expansion and boundary-driven velocity shear [56]. Next, it should be able to be extended to diatomic and polyatomic

gases and high-temperature gas flows with vibrational modes or chemical reactions and unsteady flow problems. Lastly, it must be developed to handle two-dimensional and three-dimensional flow problems beyond the one-dimensional flow considered in the present study. We hope to report on our progress on these challenging topics in due course.

ACKNOWLEDGEMENTS

This work was supported by the US Air Force Office of Scientific Research (AFOSR) Grant No. FA2386-22-1-4051. The authors would like to acknowledge the input of Dr. Jyothi P. Panda. The authors thank the reviewers of this article for their valuable and helpful comments.

DATA AVAILABILITY

The data that support the findings of this study are available from the corresponding author upon request.

REFERENCES

[1] R.S. Myong, Thermodynamically consistent hydrodynamic computational models for high-Knudsen-number gas flows, Physics of Fluids 11 (1999) 2788-2802.
[2] R.S. Myong, On the high Mach number shock structure singularity caused by overreach of Maxwellian molecules, Physics of Fluids 26 (2014).
[3] N.T.P. Le, H. Xiao, R.S. Myong, A triangular discontinuous Galerkin method for non-Newtonian implicit constitutive models of rarefied and microscale gases, Journal of Computational Physics 273 (2014) 160-184.
[4] A. Rana, R. Ravichandran, J.H. Park, R.S. Myong, Microscopic molecular dynamics characterization of the second-order non-Navier-Fourier constitutive laws in the Poiseuille gas flow, Physics of Fluids 28 (2016).
[5] S. Singh, A. Karchani, T. Chourushi, R.S. Myong, A three-dimensional modal discontinuous Galerkin method for the second-order Boltzmann-Curtiss-based constitutive model of rarefied and microscale gas flows, Journal of Computational Physics 457 (2022) 111052.
[6] O. Ejtehadi, R.S. Myong, I. Sohn, B.J. Kim, Full continuum approach for simulating plume-surface interaction in planetary landings, Physics of Fluids 35 (2023).
[7] T.K. Mankodi, O. Ejtehadi, T. Chourushi, A. Rahimi, R.S. Myong, nccrFOAM suite: Nonlinear coupled constitutive relation solver in the OpenFOAM framework for rarefied and microscale gas flows with vibrational non-equilibrium, Computer Physics Communications 296 (2024) 109024.

[8] Z. Jiang, W. Zhao, Z. Yuan, W. Chen, R.S. Myong, Computation of hypersonic flows over flying configurations using a nonlinear constitutive model, AIAA Journal 57 (2019) 5252-5268.
[9] T.K. Mankodi, R.S. Myong, Quasi-classical trajectory-based non-equilibrium chemical reaction models for hypersonic air flows, Physics of Fluids 31 (2019).
[10] T.K. Mankodi, R.S. Myong, Erratum: "Quasi-classical trajectory-based non-equilibrium chemical reaction models for hypersonic air flows" [Phys. Fluids 31, 106102 (2019)], Physics of Fluids 32 (2020).
[11] L.V. Ballestra, R. Sacco, Numerical problems in semiconductor simulation using the hydrodynamic model: a second-order finite difference scheme, Journal of Computational Physics 195 (2004) 320-340.
[12] S.K. Blau, Conduction electrons flow like honey, Physics Today 70 (2017) 22-22.
[13] N. Cagney, S. Balabani, Taylor-Couette flow of shear-thinning fluids, Physics of Fluids 31 (2019).
[14] R. Evans, D. Frenkel, M. Dijkstra, From simple liquids to colloids and soft matter, Physics Today 72 (2019) 38-39.
[15] G.A. Bird, Approach to translational equilibrium in a rigid sphere gas, Physics of Fluids 6 (1963) 1518-1519.
[16] G.A. Bird, Molecular Gas Dynamics and the Direct Simulation of Gas Flows, Clarendon Press, 1994.
[17] G.A. Bird, M.A. Gallis, J.R. Torczynski, D.J. Rader, Accuracy and efficiency of the sophisticated direct simulation Monte Carlo algorithm for simulating noncontinuum gas flows, Physics of Fluids 21 (2009).
[18] R.S. Myong, A. Karchani, O. Ejtehadi, A review and perspective on a convergence analysis of the direct simulation Monte Carlo and solution verification, Physics of Fluids 31 (2019).
[19] A. Karchani, R.S. Myong, Convergence analysis of the direct simulation Monte Carlo based on the physical laws of conservation, Computers & Fluids 115 (2015) 98-114.
[20] I.D. Boyd, G. Chen, G.V. Candler, Predicting failure of the continuum fluid equations in transitional hypersonic flows, Physics of Fluids 7 (1995) 210-219.
[21] T.E. Schwartzentruber, I.D. Boyd, Progress and future prospects for particle-based simulation of hypersonic flow, Progress in Aerospace Sciences 72 (2015) 66-79.
[22] E. Jun, I.D. Boyd, Assessment of the LD-DSMC hybrid method for hypersonic rarefied flow, Computers & Fluids 166 (2018) 123-138.
[23] S. Mallikarjun, V. Casseau, W.G. Habashi, S. Gao, A. Karchani, Hybrid Navier–Stokes–direct simulation Monte Carlo automatic mesh optimization for hypersonics, Journal of Thermophysics and Heat Transfer 37 (2023) 779-806.
[24] P.L. Bhatnagar, E.P. Gross, M. Krook, A model for collision processes in gases. I. Small amplitude processes in charged and neutral one-component systems, Physical Review 94 (1954) 511-525.
[25] E.M. Shakhov, Generalization of the Krook kinetic relaxation equation, Fluid Dynamics 3 (1968) 95-96.
[26] L.H. Holway, Jr., New statistical models for kinetic theory: Methods of construction, Physics of Fluids 9 (1966) 1658-1673.
[27] D. Burnett, The distribution of molecular velocities and the mean motion in a non-uniform gas, Proceedings of the London Mathematical Society s2-40 (1936) 382-435.
[28] C.J. Greenshields, J.M. Reese, The structure of shock waves as a test of Brenner's modifications to the Navier–Stokes equations, Journal of Fluid Mechanics 580 (2007) 407-429.

[29] A. Agrawal, A. Gavasane, R.S. Jadhav, Improved theory for shock waves using the OBurnett equations, Journal of Fluid Mechanics 929 (2021) A37.
[30] H. Grad, On the kinetic theory of rarefied gases, Communications on Pure and Applied Mathematics 2 (1949) 331-407.
[31] H. Struchtrup, M. Torrilhon, Regularization of Grad's 13 moment equations: Derivation and linear analysis, Physics of Fluids 15 (2003) 2668-2680.
[32] D.R. Emerson, X.-J. Gu, A high-order moment approach for capturing non-equilibrium phenomena in the transition regime, Journal of Fluid Mechanics 636 (2009) 177-216.
[33] B.C. Eu, Kinetic Theory and Irreversible Thermodynamics, Wiley, 1992.
[34] R.S. Myong, A computational method for Eu's generalized hydrodynamic equations of rarefied and microscale gasdynamics, Journal of Computational Physics 168 (2001) 47-72.
[35] R.S. Myong, A generalized hydrodynamic computational model for rarefied and microscale diatomic gas flows, Journal of Computational Physics 195 (2004) 655-676.
[36] J. Sirignano, J.F. MacArt, Deep learning closure models for large-eddy simulation of flows around bluff bodies, Journal of Fluid Mechanics 966 (2023) A26.
[37] K. Duraisamy, G. Iaccarino, H. Xiao, Turbulence modeling in the age of data, Annual review of fluid mechanics 51 (2019) 357-377.
[38] H. Xiao, J.L. Wu, J.X. Wang, R. Sun, C.J. Roy, Quantifying and reducing model-form uncertainties in Reynolds-averaged Navier–Stokes simulations: A data-driven, physics-informed Bayesian approach, Journal of Computational Physics 324 (2016) 115-136.
[39] A. Kurzawski, J. Ling, J. Templeton, Reynolds averaged turbulence modelling using deep neural networks with embedded invariance, Journal of Fluid Mechanics 807 (2016) 155-166.
[40] J. Zhang, W. Ma, Data-driven discovery of governing equations for fluid dynamics based on molecular simulation, Journal of Fluid Mechanics 892 (2020) A5.
[41] S.H. Rudy, S.L. Brunton, J.L. Proctor, J.N. Kutz, Data-driven discovery of partial differential equations, Science Advances 3 (2017) e1602614.
[42] H. Xing, J. Zhang, W. Ma, D. Wen, Using gene expression programming to discover macroscopic governing equations hidden in the data of molecular simulations, Physics of Fluids 34 (2022).
[43] S. Yao, W. Zhao, C. Wu, W. Chen, Nonlinear constitutive calculation method of rarefied flow based on deep convolution neural networks, Physics of Fluids 35 (2023).
[44] W. Zhao, L. Jiang, S. Yao, W. Chen, Data-driven nonlinear constitutive relations for rarefied flow computations, Advances in Aerodynamics 3 (2021) 1-19.
[45] A.S. Nair, J. Sirignano, M. Panesi, J.F. MacArt, Deep learning closure of the Navier–Stokes equations for transition-continuum flows, AIAA Journal (2023) 1-14.
[46] J.D. Anderson, Modern Compressible Flow with Historical Perspective, McGraw-Hill, 1982.
[47] M. Morduchow, P.A. Libby, On a complete solution of the one-dimensional flow equations of a viscous, heat-conducting, compressible gas, Journal of the Aeronautical Sciences 16 (1949) 674-684.
[48] H. Grad, The profile of a steady plane shock wave, Communications on Pure and Applied Mathematics 5 (1952) 257-300.
[49] H.M. Mott-Smith, The solution of the Boltzmann equation for a shock wave, Physical Review 82 (1951) 885-892.
[50] M. Al-Ghoul, B.C. Eu, Generalized hydrodynamics and shock waves, Physical Review E 56 (1997) 2981-2992.

[51] R.S. Myong, Analytical solutions of shock structure thickness and asymmetry in Navier–Stokes/Fourier framework, AIAA Journal 52 (2014) 1075-1081.
[52] B. van Leer, Towards the ultimate conservative difference scheme, Journal of Computational Physics 135 (1997) 229-248.
[53] E.F. Toro, M. Spruce, W. Speares, Restoration of the contact surface in the HLL-Riemann solver, Shock Waves 4 (1994) 25-34.
[54] H.K. Moffatt, G.M. Zaslavsky, P. Comte, M. Tabor, Topological Aspects of the Dynamics of Fluids and Plasmas, Springer Netherlands, 2013.
[55] S. Singh, A. Karchani, K. Sharma, R.S. Myong, Topology of the second-order constitutive model based on the Boltzmann–Curtiss kinetic equation for diatomic and polyatomic gases, Physics of Fluids 32 (2020).
[56] T.K. Mankodi, R.S. Myong, Boltzmann-based second-order constitutive models of diatomic and polyatomic gases including the vibrational mode, Physics of Fluids 32 (2020).